Available online at www.sciencedirect.com
SCIENCE DIRECT®
Journal of Magnetic Resonance 171 (2004) 162–169
JMR Journal of Magnetic Resonance
www.elsevier.com/locate/jmr

Communication

Ultrafast 2D NMR spectroscopy using a continuous spatial encoding of the spin interactions

Yoav Shrot, Boaz Shapira, Lucio Frydman*

Department of Chemical Physics, Weizmann Institute of Science, 76100 Rehovot, Israel

Received 2 June 2004

Abstract

A new protocol for acquiring multidimensional NMR spectra within a single scan is introduced and illustrated. The approach relies on applying a pair of frequency-chirped excitation and storage pulses in combination with echoing magnetic field gradients, in order to impart the kind of linear spatial encoding of the NMR interactions that is required by ultrafast 2D NMR spectroscopy. It is found that when dealing with 2D NMR experiments involving a t_1 amplitude-modulation of the spin evolution, such continuous encoding scheme presents a number of advantages over alternatives employing discrete excitation pulses. From an experimental standpoint this is mainly reflected by the use of a single pair of bipolar gradients during the course of the indirect-domain encoding, as opposed to the numerous (and more intense) gradient echoes required so far. In terms of the spectral outcome, main advantages of the continuous spatial encoding scheme are the avoidance of ''ghost peaks'' and of ''enveloping effects'' associated to the discrete excitation mode. The principles underlying this new spatial encoding protocol are derived, and its applicability is demonstrated with homo- and heteronuclear 2D ultrafast NMR applications on small molecule and on protein samples.

Keywords: Ultrafast 2D NMR; Spatial encoding; Chirped RF irradiation; Protein HSQC NMR

1. Introduction

Two-dimensional spectroscopy plays a central role in most chemical and biochemical applications involving the use of Nuclear Magnetic Resonance [1,2]. The majority of 2D NMR experiments carried out within analytical settings rely on the paradigm put forward by Jeener, Ernst, and co-workers [3,4] whereby the effects of the initial Ω_1 interactions are indirectly monitored by incrementing an associated time parameter t_1, while the second set of frequencies Ω_2 becomes directly encoded by an acquisition time t_2. The step-wise nature by which t_1 values are incremented in this protocol implies that, even when dealing with experiments characterized by ample sensitivity, numerous individual scans will have to be collected for the sake of appropriately sampling the indirect time-domain. During recent years a number of initiatives have been launched to alleviate this limitation [5–10]. Among these proposals counts an ''ultrafast'' approach that departs from the canonical sampling mode, and enables the acquisition of generic nD NMR spectra within a single scan [10–12]. At the heart of this new approach lies replacing the temporal t_1 encoding employed in traditional 2D NMR experiments by an analogous spatial encoding of the spin interactions; i.e., replacing the customary $\Omega_1 \cdot t_1$ indirect-domain evolution with a spatially dependent evolution phase of the form $C\Omega_1 \cdot z$. The winding of spin coherences created by such spatial encoding procedure will be preserved throughout the mixing period of a 2D NMR sequence—usually in the form of an amplitude modulation—and can be subsequently probed by the action of a field gradient G_a. This acquisition gradi-

* Corresponding author. Fax: +972 8 9344123.
E-mail address: lucio.frydman@weizmann.ac.il (L. Frydman).

1090-7807/$ - see front matter © 2004 Elsevier Inc. All rights reserved.
doi:10.1016/j.jmr.2004.08.001

ent will unravel the spatial encoding that was created prior to the mixing period, and lead whenever $k = \gamma_a \int_0^t G_a(t')\,dt' = C\Omega_1$ to site-specific echoes whose observation will reveal the nature of the internal spin evolution frequencies. Furthermore, this gradient-driven readout can be undone and reapplied numerous times during the course of an acquisition simply by oscillating the sign of the applied G_a gradient, allowing one to monitor the direct-domain Ω_2 frequencies via the phase modulations that they will impart on the multiple k-domain echoes then resulting as a function of t_2.

It follows from this summary that an important component in the successful implementation of ultrafast nD NMR experiments resides in imparting a suitable spatial encoding, reflecting as $C\Omega_1 \cdot z$ the nature of the internal spin interactions. A number of alternatives have been discussed in the literature to achieve this aim. Our initial proposal employed a series of discrete frequency-shifted excitation pulses that, when applied in combination with bipolar gradient echoes, will deliver the desired encoding profile for either phase- or amplitude-modulated 2D NMR experiments (Fig. 1A, [10]). Constant-time 2D alternatives involving either trains of discrete radiofrequency (RF) π pulses or adiabatic sweeps in combination with bipolar gradients have also been proposed to achieve such goal [11–13]. More recently, and within the context of exploiting the ultrafast NMR principle for the sake of collecting 2D magnetic resonance images, we began exploring the possibility of relying on excitation pulses whose frequencies are continuously swept—so-called chirped-RF excitation pulses [14]. As discussed in the present Communication we find that combining two such frequency-swept nutation pulses with a suitable bipolar gradient echo, enables one to store amplitude-modulated states possessing the linear z and Ω_1 dependencies required by ultrafast 2D NMR spectroscopy. It is then demonstrated that, in addition to imposing fewer demands on the NMR hardware than the discrete RF excitation mode, such chirped irradiation scheme can help remove a number of spectral artifacts associated with the discrete excitation proposal. All this can be achieved without incurring on sensitivity penalties when considering amplitude-modulated experiments on non-diffusing samples, thus yielding a tool that is applicable to a majority of 2D NMR correlation sequences. The following paragraphs introduce, exemplify, and discuss in further detail, this new approach to spatial encoding and to ultrafast 2D NMR.

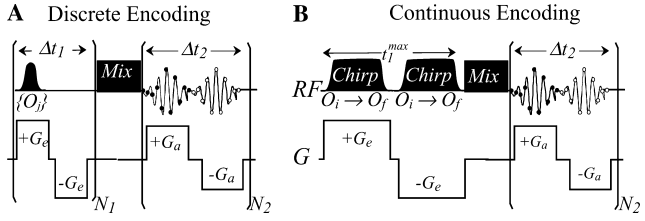

Fig. 1. Comparison between two schemes capable of creating the kind of spatially encoded spin states demanded for the execution of amplitude-modulated 2D NMR spectroscopy within a single scan. (A) Original protocol whereby indirect-domain Ω_1 interactions are encoded by a discrete train of N_1 RF pulses, applied at constant frequency increments ΔO and spaced by constant delays Δt_1. Each excitation pulse is applied in combination with its own $\pm G_e$ excitation gradient echo; following the mixing process interactions are decoded using an oscillatory $\pm G_a$ acquisition gradient. (B) New scheme discussed in this work whereby the train of excitation pulses/gradient echoes in scheme (A) is replaced by a pair of continuous irradiation pulses in combination with a single bipolar gradient. Although both RF pulses are here identical the purpose of the first of these RF sweeps is to sequentially excite spins throughout the sample, whilst the purpose of the second one is to store the t_1-encoded coherences. See the text for additional details.

2. Spatially encoded 2D NMR using chirped RF pulses

The new scheme introduced in this work pertains to experiments where the indirect-domain spin evolution is encoded as an amplitude modulation; that is, it concerns the extensive family of 2D correlation NMR pulse sequences where t_1 events become triggered and concluded by RF pulses which retain a well-defined projection of the evolving spin coherences [1]. The generic new scheme that we would like to discuss for imposing on the excitation/storage combinations underlying such pulse sequences the linear spatial encoding required by ultrafast 2D NMR, is depicted in Fig. 1B. On comparing this protocol with the counterpart which we have been employing so far (Fig. 1A), one can appreciate that the new variant replaces the original train of discrete frequency-shifted RF excitation pulses by two identical chirped RF pulses: an "excitation" irradiation applied while in the presence of a gradient $+G_e$, and a "storage" sweep applied while subjecting the spins to a reversed gradient $-G_e$. The purpose of the initial chirp pulse is to excite as fully as possible from initial longitudinal S-spin states—either S_z magnetizations or $2I_\alpha S_z$ multiple-spin terms—the transverse S coherences that will evolve over the course of t_1. A key factor defining the efficiency of this excitation process will thus be the adiabaticity parameter $\alpha = |(\Omega_{RF})^2/R|$, given by the ratio between the nutation frequency Ω_{RF} imparted by the RF, and the rate $R = \frac{\partial O}{\partial \tau}$ characterizing how rapidly the RF offset O is swept during the course of the frequency chirp [15]. An efficient excitation will be characterized by α parameters that are neither too small nor too large—conditions corresponding to the sudden passage and to the adiabatic inversion regimes, respectively, where little actual excitation can be achieved. As discussed elsewhere in further detail, the condition that maximizes a transverse rotation of single-spin coherences is given by an adiabaticity parameter $\alpha \approx 0.068$ [14]. In frequency units this translates as $(\Omega_{RF})_{opt} \approx 0.26\sqrt{R}$;

numerical simulations show that RF field strengths matching in this manner the rates involved in the chirping, execute essentially complete $\pi/2$ nutations on any spin resonating over the range of offsets being swept. As for the second pulse mentioned in Fig. 1B, the one whose purpose is to store the coherences that have been precessing over the course of t_1 back into longitudinal spin states, it is clear that its goal will also involve sequential $\pi/2$ spin nutations over the relevant frequency bandwidth. It follows that an adiabaticity parameter $\alpha \approx 0.068$ will once again be best suited for this purpose, and that exactly the same chirp pulses are to be applied over the course of the $+G_e$ excitation as during the course of the $-G_e$ storage processes.

Having defined the requirements that the RF pulses have to fulfill for an efficient excitation and storage of the spin coherences, we discuss next how the scheme introduced in Fig. 1B succeeds in imparting the desired t_1 modulation reflecting solely the internal interaction frequencies Ω_1 and varying linearly with z position. In order to simplify this description we shall neglect at this stage the influence that chemical shifts may actually have on the instant at which spins are addressed by the RF, and assume that at a given time τ over the course of the frequency sweeps the consequence of the pulses will be to either excite or store all spins placed at a particular coordinate fulfilling $O(\tau) = \gamma_e \mathbf{G} \cdot z$. Furthermore, we shall assume that the applied RF sweeps affect all spins within a spatial confine L, by proceeding at a constant rate between initial and final offset values $O_i = -O_f = |\gamma_e G_e L/2|$. Then, since identical $O_i \to O_f$ sweep directions but opposite $+G_e/-G_e$ field gradients define the commencement and the conclusion of the t_1 period, spins positioned at the first z coordinates to become excited will also be the last spins to have their transverse coherences stored (Fig. 2). Conversely, spins at the opposite end of the sample will experience the least evolution both during the course of the excitation as well as of the storage sweeps. In general it follows that for spins at arbitrary z positions, this scheme will impart equal free evolution times t_1^+ during the course of the "excitation" RF sweep, as free evolution times t_1^- are allowed over the extent of the "storage" sweep. The effects imparted by the $+G_e/-G_e$ field gradients will consequently cancel away over the total $t_1 = t_1^+ + t_1^-$ evolution time, while those of the internal Ω_1 interactions accumulate unhindered over the same interval. On considering further that the τ-linearity with which both $O_i \to O_f$ sweeps proceeded made the extent of the t_1 evolution proportional to z for every sample coordinate, one can appreciate why the overall effect imparted on the spin states prior to the mixing ends up involving the desired $C\Omega_1 \cdot z$ modulation yet no influences from the external field gradients.

A rigorous derivation of how the sequence depicted in Fig. 1B achieves its encoding requires computing the actual times t_1^+, t_1^- evolved by spins under arbitrary conditions, as well as accounting for the various sources that will affect the phase evolution accumulated by the spins during the course of the experiment. To carry out such derivation we extend our recent analysis on chirp-based single-scan 2D MR imaging procedures [14] to the spectroscopy case being addressed in this work, and begin by calculating the relation between the free evolution times allotted to the spins by the initial excitation and subsequent storage RF sweeps, and their spatial coordinate z. Extending the arguments in the previous paragraph (Fig. 2) we shall assume that these delays $t_1^+(z)$, $t_1^-(z)$ are defined by the instant τ at which the frequency offset of a chirped RF pulse adopts a value

$$O(\tau_\pm) = \pm\gamma_e G_e z + \Omega_1, \tag{1}$$

where Ω_1 is an internal frequency shift and the signs depend on whether the excitation or the storage processes are being considered. Bearing in mind that pulses are swept from initial O_i to final O_f frequencies at a constant rate R—$O(\tau) = O_i + R\tau$—and that the on-resonance condition in Eq. (1) will trigger the evolution over the excitation sweep but conclude it over the storage period, it follows that the consecutive free evolution times being sought will be given by

$$t_1^+(z) = \frac{O_f - O_i}{R} - \tau_+(z) = \frac{O_f - \gamma_e G_e z - \Omega_1}{R} \tag{2a}$$

and

$$t_1^-(z) = \tau_-(z) = \frac{-O_i - \gamma_e G_e z + \Omega_1}{R}. \tag{2b}$$

With these definitions it is possible to calculate the overall phase accumulated by spins at a particular z

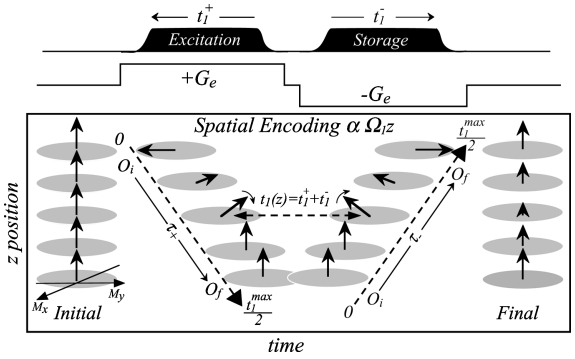

Fig. 2. Simplified description of the effects introduced by pre-mixing events in the pulse sequence shown in Fig. 1B, on the spins' evolution. RF offsets O are assumed swept between an initial value O_i and a final value $O_f = -O_i$ at a constant rate R during both the "excitation" ($+G_e$) and the "storage" ($-G_e$) portions of the sequence. For either the excitation or storage sweeps the RF will nutate by 90° spins whose z positions fulfill the $O(\tau_\pm) = O_i + R\tau_\pm = \pm\gamma_e G_e z$ condition, as illustrated for the center spin-packet. The evolution time t_1^+ undergone by spin coherences during the course of the excitation sweep becomes then identical to the t_1^- free evolution period experienced over the storage sweep, for every z coordinate in the sample. This results in an $\Omega_1 z$ dependence for the amplitude-modulated spin states stored at the conclusion of the sequence.

coordinate during the course of the combined evolution time $t_1(z) = t_1^+(z) + t_1^-(z)$.[1] Such calculation requires in turn accounting for: (i) the precession $\phi_{\text{grad}}(t_1) = \gamma_e \int_{t_1} G(t')\,dt' \cdot z$ imposed by the action of the $\pm G_e$ external field gradients over t_1, (ii) the contribution $\phi_{\Omega_1}(t_1) = \Omega_1 \cdot t_1$ resulting from the internal spin interactions, and (iii) the additional phase that the RF-driven excitation and storage nutations will pass on to the spins due to the fact that chirped RF pulses undergo an unavoidable phase incrementation during the course of their sweeps: $\phi_{\text{pulse}}(\tau) = \int_0^\tau O(t')\,dt'$. In order to properly describe this last effect we notice that whereas on excitation at an instant τ_+ RF phase terms will impart themselves onto the spins, upon storing a particular coherence at a latter time τ_- these terms will actually provide a reference against which the overall dynamic evolution phase accrued by the spins is to be compared. Taking these various issues as well as the definitions given in Eqs. (2a) and (2b) into consideration, results in an overall phase expression

$$\Phi[t_1(z)] = \phi_{\Omega_1}[t_1(z)] + \phi_{\text{grad}}[t_1(z)] + \Delta\phi_{\text{pulse}}[t_1(z)], \tag{3}$$

where

$$\begin{aligned}\phi_{\Omega_1}[t_1(z)] &= \Omega_1\left(t_1^+ + t_1^-\right)\\ &= \Omega_1\left(\frac{O_f - O_i}{R}\right) - \Omega_1\left(\frac{2\gamma_e G_e}{R}\right)z,\end{aligned} \tag{4a}$$

$$\begin{aligned}\phi_{\text{grad}}[t_1(z)] &= (+\gamma_e G_e z)t_1^+ + (-\gamma_e G_e z)t_1^-\\ &= \gamma_e G_e z\left(\frac{O_f + O_i}{R}\right) - \Omega_1\left(\frac{2\gamma_e G_e}{R}\right)z,\end{aligned} \tag{4b}$$

and

$$\begin{aligned}\Delta\phi_{\text{pulse}}[t_1(z)] &= \int_0^{\tau_+} O(t')\,dt' - \int_0^{\tau_-} O(t')\,dt'\\ &= \int_{t_1^-}^{\frac{t_1^{\max}}{2} - t_1^+} [O_i + R \cdot t']\,dt'\\ &= \Omega_1\left(\frac{2\gamma_e G_e}{R}\right)z.\end{aligned} \tag{4c}$$

The overall spatial dependence of Eq. (3) can therefore be summarized as

$$\Phi(z) = \Omega_1\left(\frac{O_f - O_i}{R}\right) - 2\frac{\gamma_e G_e}{R}\left[\Omega_1 - \left(\frac{O_f + O_i}{2}\right)\right]z. \tag{5}$$

Considering further that an arbitrary shift $\Delta\theta$ can also be imposed between the phases of the excitation and storage chirp pulses, and that the latter will only preserve an orthogonal projection of the evolving coherences, it follows that the overall amplitude-modulated signal resulting at the conclusion of the double-sweep procedure schematized in Fig. 1B will be

$$S(z) \propto A(z) \cdot \cos[\Phi(z) + \Delta\theta]. \tag{6}$$

$A(z)$ defines here a relative intensity profile for the site in question as a function of position z, suitably weighted by the spin relaxation and the translational diffusion which may have occurred over the course of $t_1(z)$. On judging these last two expressions, it is clear that the pulse sequence introduced in Fig. 1B succeeds to impose the linear spatial amplitude-modulation that we set out to obtain.

Before concluding this section it is enlightening to compare the results summarized in Eq. (5), with the phase behavior that we have previously derived for spatially encoded experiments involving discrete excitation pulses [11]. One of the features associated to these prior calculations was a first-order phase distortion, stemming from the fact that the $z = 0$ origin of the spatial encoding corresponded with an evolution instant $t_1 \approx t_1^{\max}/2$ that was different from zero. Considering that according to the scheme in Fig. 2 $(O_f - O_i)/R \approx t_1^{\max}/2$, it is clear that the first term in Eq. (5) reflects an identical phase shift that will also in this case pass onwards as a first-order phase distortion of the indirect-domain peaks. Also in common with the discrete excitation scheme is the $(O_f + O_i)/2$ term in Eq. (5); as mentioned O_f is usually set to $-O_i$, but when this is not the case such term will define a reference frequency with respect to which echoes along the k/v_1 axis will appear defined. $(O_f + O_i)/2$ consequently plays the role of an offset value, that can be manipulated to bring peaks into the desired indirect-domain spectral window. A final important factor to compare is the spatio-temporal ratio C, relating the echo positions observed along the k/v_1 axis with the corresponding Ω_1 indirect-domain frequency values. As may be recalled this coefficient took in the discrete excitation case a value $C = \Delta t_1 \gamma_e G_e/\Delta O$; considering that in the continuous encoding sequence R plays a role analogous to $\frac{\Delta O}{\Delta t_1}$, it follows from the $-2\gamma_e G_e/R$ factor scaling $\Omega_1 \cdot z$ in Eq. (5) that the encoding can now be considered twice as efficient as in the previously discussed case. This in turn reflects the fact that in the amplitude-modulated scheme hereby discussed frequency-selective pulses are applied during the course of both the excitation as well as the storage processes—as opposed to solely over the course of the excitation, cf. Fig. 1A; thereby the net t_1 dependence of the spatial encoding becomes doubled. The ensuing spatio-temporal ratio also enables an estimation of the spectral range that a constant acquisition gradient G_a acting over a time period T_a will succeed in unraveling: the indirect-domain spectral width for experiments of the kind described in Fig. 1B will be $SW_1 = |k_{\text{acq}}^{\max}/C| = |(R\gamma_a G_a T_a)/(2\gamma_e G_e)|$.

[1] A transition time Δ between t_1^+ and t_1^- will in general also be required for performing the $+G_e \to -G_e$ transition, inserting decoupling π pulses, etc. Usually $\Delta \ll t_1^+, t_1^-$ and its effects can be disregarded, yet even when this is not the case the final form of the spatial encoding is as described in this paragraph.

3. Results

The generality of the scheme just presented is demonstrated in this section with two independent ultrafast 2D NMR tests. One of these involved a homonuclear 2D TOCSY ^{1}H NMR acquisition, collected on a Varian iNova 500 MHz NMR spectrometer equipped with an inverse probehead as platform. The pulse sequence employed in this experiment is illustrated on the top portion of Fig. 3. It consisted of an initial pair of chirped excitation/storage RF pulses applied in the presence of z bipolar gradients to impose the desired longitudinal spatial encoding, a 40 ms long isotropic mixing sequence whose purpose was to transfer among mutually coupled spins the magnetizations thus stored, and a final $\pi/2$ pulse followed by an oscillating $\pm G_a$ gradient for the sake of unraveling the nature of the pre- and post-mixing evolution frequencies. Data points were collected over the course of this $\pm G_a$ gradient application in the usual ultrafast NMR rapid-sampling fashion [10,11], then sorted out according to their k/v_1 values and Fourier transformed as a function of t_2 for the sake of retrieving the desired 2D NMR spectrum. The lower panel of Fig. 3 illustrates results arising from this single-scan procedure using a 20 mM n-butylchloride/$CDCl_3$ sample as example; the quality and correctness of the 2D NMR data obtained at the conclusion of the process are evident.

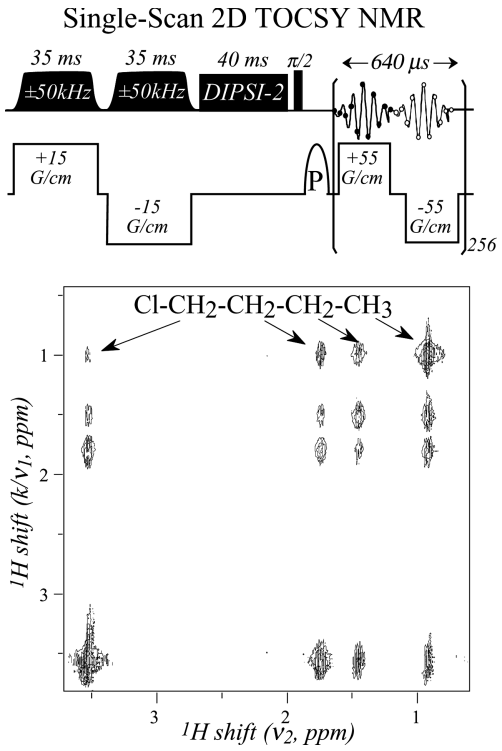

Fig. 3. Single-scan 2D TOCSY NMR spectrum acquired on an n-butylchloride/$CDCl_3$ sample, utilizing a sequence like the one illustrated on Fig. 1B with the following parameters: $G_e = 15$ G/cm, $O_i = -O_f = 50$ kHz, $t_1^{max} = 70$ ms, $G_a = 55$ G/cm, $N_2 = 256$, $T_a = 0.31$ ms sampled with a constant dwell of 2 μs, and a ±210 kHz filter bandwidth (derived from $\pm\gamma_a G_a L/2$; L being the sample length). All gradient-switching times were set to 10 μs, and a 100 μs purging gradient pulse (P) was applied just prior to beginning data digitization in order to clean up undesired residual signals. The frequency-chirped RF pulses involved in this sequence were programmed in real time using the Pbox Varian software package, with a WURST-50 amplitude-modulated pulse shape, an adiabaticity parameter $\alpha \approx 0.068$, and a 2 μs digital resolution. A 40 ms long DIPSI-2 type sequence, applied in the absence of gradients and over a 10 kHz bandwidth, was employed for the mixing. The acquired data points were separated for their off-line processing into $+G_a$ and $-G_a$ contributions [10]; the contour plot illustrated in (B) then resulted from subjecting one of these sets to a suitable shearing, zero-filling to 256×512 (k, t_2)-points, Fourier transformation against t_2, and magnitude mode calculation.

The second test to be discussed involved a 2D ^{1}H–^{13}C HSQC NMR acquisition on a uniformly ^{13}C enriched sample: protein A, a 10 kDa biopolymer kindly provided to us by Dr. S. Freund (Cambridge University, UK). This sample was dissolved at a 3.75 mM concentration in a 20 mM sodium acetate/D_2O buffer, loaded into a 5 mm Shigemi NMR tube, and examined on a Bruker Avance 800 MHz NMR spectrometer using the pulse sequence illustrated in Fig. 4A. Such sequence is akin to the ultrafast 2D HSQC experiment we have presented elsewhere [11], apart from the fact that it replaces the discrete train of frequency-shifted RF pulses by a single pair of chirped pulses for encoding the heteronuclear evolution. A single ^{1}H π pulse was also inserted in between the excitation and storage pulses in order to achieve a fully decoupled ^{13}C t_1 evolution; selective ^{13}C carbonyl π pulses were also assayed, but did not result in a significant resolution enhancement and their use was thus discontinued. Unlike the case for the acquisition reported in Fig. 3 two scans—differing by a 180° phase shift of the initial excitation chirp pulse and of the final receiver demodulation—were collected during the course of these protein 2D ultrafast NMR experiments. This was not done to enhance spectral sensitivity, but to achieve a more complete suppression of the otherwise intense residual HDO solvent peak. Figs. 4B–D summarize some of the results obtained during the course of these tests. Shown in the first of these insets is a conventional 2D ^{1}H–^{13}C HSQC spectrum, focusing on the aliphatic protein resonances appearing in the 10–70 ppm ^{13}C region. Though spectral widths in this experiment were chosen so as to result in a folding of the C_α resonances, resolution of the various peaks under such acquisition conditions was not problematic. Shown in Fig. 4C is a similar spectrum, recorded this time using the chirped-RF ultrafast HSQC sequence. Although resolution is here somewhat poorer than in the conventional counterpart, the identification of the various individual resonances is still straightforward. The lower resolution observed in this 2D plot actually stemmed from limitations in the strength of the gradient system available for this study, when trying to cover the spectral

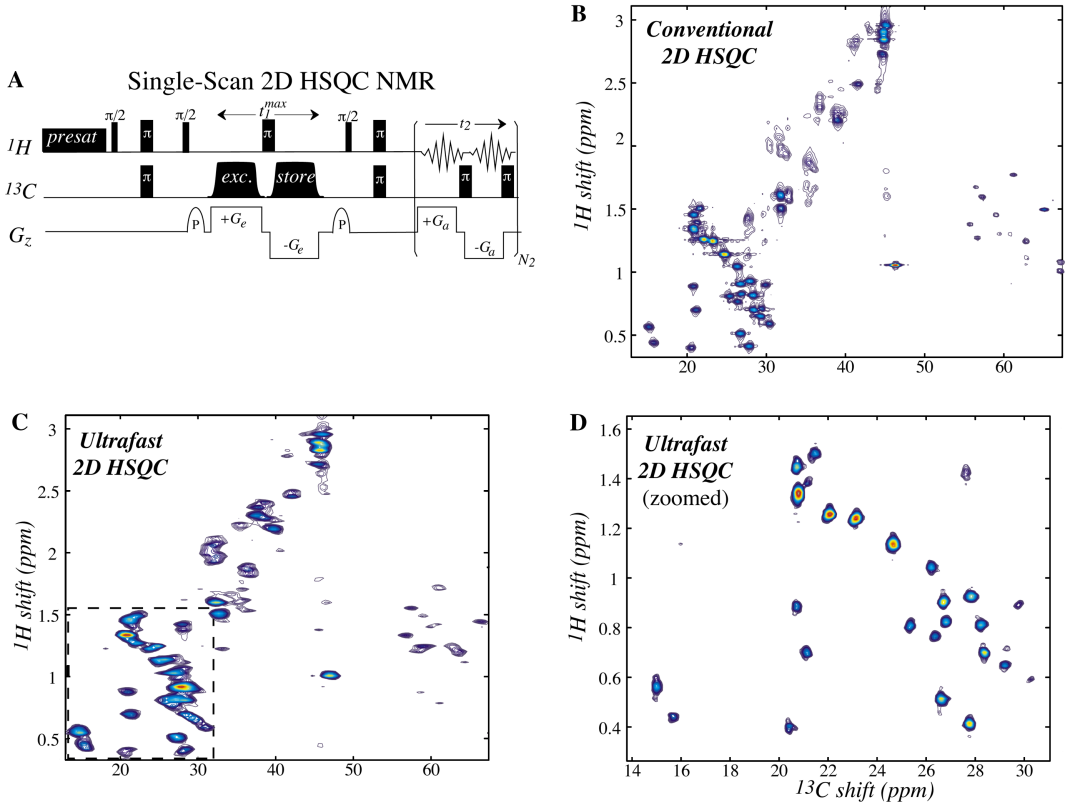

Fig. 4. Summary of the ultrafast 2D heteronuclear NMR results obtained at 800 MHz utilizing the sequence illustrated on (A), when applied to a lyophilized protein A sample dissolved in D_2O at 25 °C. (B) Conventional 2D ^1H–^{13}C HSQC NMR experiment arising from the acquisition of 128 t_1 increments, each of them involving eight phase-cycled scans (plus 16 dummy scans) sampled with 1024 points along t_2. (C) Ultrafast 2D HSQC results stemming from the sequence in part (A), focusing on a similar spectral window as illustrated in the conventional experiment. Only two scans differing in the phases of the initial chirped pulse and of the receiver were here collected using $G_e = 26$ G/cm, $O_i - O_f = 50$ kHz, $t_1^{max} = 4.8$ ms, $G_a = 47.5$ G/cm, $N_2 = 32$, $T_a = 0.18$ ms sampled with a physical dwell of 3 μs, 2 ms long purging (P) gradient pulses, and a 125 kHz filter bandwidth. (D) Ultrafast 2D NMR acquisition focusing on the limited spectral region indicated in (C) by the dotted rectangle, corresponding to the methyl sites in the protein. The acquisition parameters for these data included $G_e = 42$ G/cm, $O_i - O_f = 80$ kHz, $t_1^{max} = 16$ ms, $G_a = 18.4$ G/cm, $N_2 = 64$, and $T_a = 0.4$ ms. The frequency-chirped pulses in these sequences were pre-programmed using the Stdisp Bruker software package, with a 10% pulse shape smoothing, an adiabaticity parameter $\alpha \approx 0.068$, and a 1 μs digital resolution. Processing was essentially as detailed for the spectrum in Fig. 3.

width ranges a priori defined for the experimental acquisition. If such coverage requirements are eased, however, the ultrafast acquisition protocol has no problems in matching the resolution available in conventional multiscan 2D NMR acquisitions. This is exemplified in Fig. 4D, which shows an ultrafast ^1H–^{13}C HSQC acquisition focusing solely on the methyl region of the 2D NMR and characterized by a nearly optimal spectral resolution.

4. Discussion and conclusions

Having introduced and illustrated a new continuous approach to achieve the spatial encoding required by ultrafast 2D NMR, we would like to conclude by expanding our discussion on the potential benefits of this approach vis-à-vis hitherto available discrete excitation protocols. As mentioned earlier numerous basic features of the two methods are actually common: they both impart similar encodings with respect to the spatial dimension, peaks are in both cases affected by similar first-order phase distortions, and appear shifted by a similar offset-type parameter under the experimentalist's control. Furthermore, when considering nD NMR pulse sequences where the indirect evolution is imposed as an amplitude modulation, both discrete and continuous protocols will be affected in similar ways by transverse spin relaxation. Hence the various arguments derived elsewhere regarding lineshapes in ultrafast 2D NMR acquisitions [16] can be ported almost unchanged to sequences relying on the chirped-RF encoding. Also in common between both acquisition modes is the fact that the amplitude z modulation represented by Eq. (6) will result in both "encoded" and "anti-encoded" windings of the magnetizations, $e^{+iC\Omega_1(z-z_0)}$ and $e^{-iC\Omega_1(z-z_0)}$, susceptible to unwinding by the application of either $+G_a$ or $-G_a$ acquisition gradients. Hence various considerations derived on the basis of this behavior for the discrete-excitation case, including the achievement of purely

absorptive 2D NMR lineshapes, can once again be ported with minor changes to this new encoding mode [16]. Yet in spite of these several features in common, we believe that the continuous encoding mode exhibits a number of advantages over its discrete counterpart worth remarking. One of these derives from the fact that instead of the numerous gradient-switching events demanded by the discrete excitation mode, the continuous encoding approach only requires a single pair of bipolar gradients. When taken in unison with the lower G_e values it requires to cover a given SW_1 bandwidth, these two gradient-related features are bound to reduce instrumental artifacts and improve the lineshape quality along the indirect spectral domain, particularly in systems suffering from extensive eddy current effects such as cryogenically cooled probeheads and imaging systems. Two additional advantages of the continuous spatial encoding mode—which may not be evident from the theoretical derivation of Section 2, but follow from an inspection of the spectra shown in Figs. 3 and 4—relate to its avoidance of a number of artifacts that characterized the discrete spatial encoding procedure. Indeed as explained elsewhere in further detail [11] the reliance on discrete spin-packets to impose the spatial encoding results in the introduction of two main potential artifacts: "ghosting" effects, whereby the equal spacing Δz between the excited spin-packets leads to the appearance of side-peaks flanking the main k/v_1-echoes at intervals $k = (\Delta z)^{-1}$; and "enveloping" effects, whereby peak intensities along the k/v_1 domain appeared weighted by the RF profile used in the spatial excitation due to an intra-slice dephasing under the action of the gradients. By doing away with the discrete excitation altogether, the continuous excitation mode hereby introduced simultaneously manages to avoid both kinds of artifacts. Particularly valuable in this respect is the avoidance by the scheme introduced in Fig. 1B of the ghosting effects. While it is true that certain cases could arise where exploiting such effects would be advantageous—for instance when relying on this folding mechanism to observing peaks originally resonating outside the specified SW_1 window—"ghost peaks" are generally a complication worth suppressing when attempting to focus on portions of the 2D NMR spectrum [17]. This need becomes pressing when examining analytes in the presence of relatively intense residual solvent resonances, whose folding into a spectral region of interest is to be avoided. The quality of the zoomed spectral results illustrated in Fig. 4D bear witness to the fact that these effects cease to be a complication when relying on the chirped-RF encoding mode.

This study, together with previous developments by Pelupessy [13], present but two examples of the variations that can be imparted on the original way proposed to carry out the spatial encoding required by ultrafast 2D NMR. Such improvements are made possible by the flexibility afforded by magnetic field gradients introducing controlled inhomogeneities into an NMR sample, when applied in combination with amplitude- and phase-shaped RF irradiation schemes capable of selectively manipulating spins subject to such inhomogeneities. Further extensions of the scheme discussed in this work include departing from the application of the constant field gradients employed so far, from the linear frequency sweeps we have hereby discussed (so as to accommodate in turn the use of time-dependent gradients), from the use of a single gradient geometry (e.g., combining z and z^2 gradients to impart a continuous phase modulation in t_1), as well as including additional pulse elements in between the various spatially encoding processes in the sequence. We expect such progress to ease the realization of ultrafast nD NMR experiments in a variety of scenarios; further extensions of these ideas will constitute the topic of future studies.

Acknowledgments

We are grateful to Drs. Eriks Kupce (Varian Ltd.) and Tali Scherf (Chemical Services Department, Weizmann Institute) for their assistance in setting up the pulse sequences employed in this study. This work was supported by the Philip M. Klutznick Fund, the Minerva Foundation (Munich), the Henry Gutwirth Fund, and the Ilse Katz Magnetic Resonance Center.

References

[1] R.R. Ernst, G. Bodenhausen, A. Wokaun, Principles of Nuclear Magnetic Resonance in One and Two Dimensions, Clarendon, Oxford, 1987.
[2] J. Cavanagh, W.J. Fairbrother, A.G. Palmer III, N.J. Skelton, Protein NMR Spectroscopy: Principles and Practice, Academic Press, San Diego, 1996.
[3] J. Jeener, Lecture presented at Ampere International Summer School II, Basko Polje, Yugoslavia, September 1971.
[4] W.P. Aue, E. Bartholdi, R.R. Ernst, Two dimensional spectroscopy. Application to nuclear magnetic resonance, J. Chem. Phys. 64 (1976) 2229–2246.
[5] V.A. Mandelshtam, FDM: the filter diagonalization method for data processing in NMR experiments, Progr. NMR Spectrosc. 38 (2001) 159–196.
[6] K. Ding, A. Gronenborn, Novel 2D triple-resonance experiments for sequential resonance assignment of proteins, J. Magn. Reson. 156 (2002) 262–268.
[7] S. Kim, T. Szyperski, GFT NMR: a new approach to rapidly obtain precise high-dimensional NMR spectral information, J. Am. Chem. Soc. 125 (2003) 1385–1393.
[8] R. Freeman, E. Kupce, New methods for fast multidimensional NMR, J. Biomol. NMR 27 (2003) 101–113.
[9] B.E. Coggins, R.A. Venters, P. Zhou, Generalized reconstruction of nD NMR spectra from multiple projections: applications to the 5D HACACONH spectrum of protein G B1 domain, J. Am. Chem. Soc. 126 (2004) 1000–1001.

[10] L. Frydman, T. Scherf, A. Lupulescu, The acquisition of multidimensional NMR spectra within a single scan, Proc. Natl. Acad. Sci. USA 99 (2002) 15858–15862.
[11] L. Frydman, A. Lupulescu, T. Scherf, Principles and features of single-scan two-dimensional NMR spectroscopy, J. Am. Chem. Soc. 125 (2003) 9204–9217.
[12] Y. Shrot, L. Frydman, Single-scan NMR spectroscopy at arbitrary dimensions, J. Am. Chem. Soc. 125 (2003) 11385–11396.
[13] P. Pelupessy, Adiabatic single-scan 2D NMR spectroscopy, J. Am. Chem. Soc. 125 (2003) 12345–12350.
[14] Y. Shrot, L. Frydman, Spatially encoded NMR and the acquisition of 2D magnetic resonance images within a single scan, J. Magn. Reson. 167 (2004) 42–48.
[15] A. Abragam, Principles of Nuclear Magnetism, Oxford University Press, Oxford, 1961 (Chapter 2).
[16] B. Shapira, A. Lupulescu, Y. Shrot, L. Frydman, Line shape considerations in ultrafast 2D NMR, J. Magn. Reson. 166 (2004) 152–164.
[17] Y. Shrot, L. Frydman, Ghost-peak suppression in ultrafast two-dimensional NMR spectroscopy, J. Magn. Reson. 164 (2003) 351–356.